Estimation of Laser Shock Peening Induced Plastic Deformation in Hastelloy-X Superalloys

S. Nath*[1], P. Shukla[1], X. Shen[1], A. Behera[2] and J. Lawrence[1]

[1]*School of Mechanical, Aerospace and Automotive Engineering, Coventry University, Coventry, CVI 2JH, UK*
[2]*Department of Metallurgical and Materials Engineering, National Institute of Technology, Rourkela, 769008, India*

The goals of the present study are to strengthen a new, Hastelloy-X superalloys by prestressing the surface with laser-plasma driven shock waves and also to quantify the effect of Laser Shock Peening (LSP) on the evolution of phase, residual stress (both through thickness and on the surface), dislocation density, and hardness of Hastelloy-X superalloys. Dislocation densities in the peened and unpeened samples were measured by Wiliamson and Smallman approach to analyze the severity of plastic deformation following LSP surface treatment. The maximum compressive residual stress measured on the peened surface of Hastelloy-X samples using incremental hole drilling technique was 850 MPa. In addition, it was found that the LSP parameters have a dominant effect in tailoring the surface hardening behavior and residual stress in Hastelloy-X superalloys.

Keywords: Laser shock peening, residual stress, incremental hole drilling, dislocation density, strain hardening

1 INTRODUCTION

Hastelloy-X is a solid solution-strengthened nickel-based superalloy with excellent oxidation resistance, formability, and high-temperature strength [1-3]. Hastelloy-X superalloys are extensively used in gas turbine engines for combustion-zone components, tail pipes, and are being considered as potential material for high-temperature gas-cooled reactor (HTGR) [4]. However, failure in these materials was reported due to intergranular attack and internal

Corresponding author's e-mail: sendsubha@gmail.com

oxidation in high-temperature gas mixtures [3, 5]. The thermal stress induced cracks are responsible for the generation of intergranular attacks and occurrence of internal oxidation in Hastelloy-X superalloys.

Laser shock peening (LSP) is a surface severe plastic deformation process which involves plastic deformation of the material by high pressure shock waves resulting from interaction of energetic laser with a material [6, 7]. The generated shock waves not only deform the material in contact plastically, but also induce compressive residual stress on the surface of the material [7-10]. The generation of compressive residual stress helps to delay the crack growth/propagation, thereby increasing the fatigue strength of the material [11, 12]. The use of LSP process has also been extended to strain harden materials' surface which increases the hardness, toughness and tribological properties of the metallic and ceramic systems [10, 13, 14].

LSP of many advanced materials have been investigated which include aluminum alloys [15- 19], nickel alloys [20-29], titanium alloys [30- 35], iron alloys [36-40], magnesium alloys [41, 42], copper alloys [43] etc. Interestingly, LSP studies have not been limited to only metallic systems, it has also been studied on non-metallic systems [13, 14]. The LSP of these conventional and advanced materials have shown to improve not only the surface hardening and fatigue strength, but also significantly contributed to the improvement of corrosion and wear resistance properties [30, 44]. Grain size reduction and surface nano-crystallizations have also been observed following LSP [19, 42]. The work carried out by Tradan *et al* [19] showed an increase in the dislocation density following LSP which was responsible for the evolution of ultra-fine grains in the near surface microstructure.

Studies on LSP of Ni-based superalloys were mostly reported on the mechanical properties and residual stress development. Gill *et al* [26] compared the effect of advanced mechanical surface treatments (laser shock peening, cavitation shotless peening and ultrasonic nanostructure modification) on IN718 SPF and investigated the process effect on residual stress development, surface hardening, microstructural evolution etc. The measured residual stress and hardness were lowest amongst all the three surface treatment processes with no signature of nano-crystallization [26]. Wang *et al* [20], however, reported grain refinement following LSP of K403 Ni alloy. The studies on LSP of Ni-based superalloys depict only on qualitative dislocation density without providing the much needed quantitative information.

The aim of the present investigation is to study the effect of LSP on the properties of Hastelloy-X superalloys and to understand the strengthening mechanisms. The study is mainly focused on studying the phase distribution/evolution, microstrain development, surface hardening behavior, and evolution of dislocation density and residual stress following LSP. Microstrain and dislocation density have been measured and critically discussed to understand the strain hardening behavior in Hastelloy-X superalloys following LSP. In-depth residual stress measurement has been carried out using incre-

TABLE 1
Nominal composition and mechanical properties of Hastelloy-X used for LSP.

Composition (wt.%)							Young's modulus (GPa)	Yield strength (MPa)	Dynamic yield strength (MPa)
Ni	Cr	Fe	C	Mo	Si	W			
Bal.	20	19.8	0.1	7	0.3	0.5	190	380	570[45]

mental hole drilling technique to quantify the depth of residual stress in the material following LSP surface treatment.

2 MATERIALS AND METHODS

2.1 Materials
LSP was carried out on rectangular Hastelloy-X superalloy samples (30 mm × 10 mm × 10 mm dimension), whose composition and mechanical properties are mentioned in Table 1. Prior to LSP, these superalloy samples were stress relieved at 1175 ºC for an hour followed by grinding in 600 µm grit size SiC papers to remove the surface residues and oxides. Ultrasonic cleaning was carried out in acetone and isopropyl alcohol baths to remove any contaminants present on the surface followed by blower drying.

2.2 Laser shock peening
In the present study, a 10 J pulsed Nd:YAG laser system (LPY10J; Litron) was used for the laser shock peening (LSP) study. The schematic of the LSP set up is shown in Fig.1. The LSP studies were carried out with a radiation wavelength of 1064 nm and a pulse duration of 8 ns long at a repetition rate of 10 Hz. The raw beam diameter was 25 mm which was then focused down to 3 - 7.5 mm on the sample's surface using a fused silica lens (focal length = 50 mm). The laser beam divergence was 0.5 mrad ($M^2 \approx 1.99$). The laser beam radiance density were measured to be between 6.44 to 22.65 $J.cm^2.Sr^{-1}$. µm [46–49]. Black polyisobutylene tape with a thickness of 500 mm was used as an absorptive layer to prevent any thermal effect on the sample during LSP process. Water with a flow rate of 2 L/min was used as a confinement medium in the present study. All the samples were treated with single shot laser pulse with an overlap of 50%. The process map adopted in the present study are presented in Figure. 2. Four different systems were developed based on the laser energy and beam diameter combinations. This led to four different laser power densities used in the present study.

   LSP involves irradiating the surface of the target using a high energy laser which then forms an expanding plasma, following laser-material interaction, with high pressure shock waves propagating into the material. The material is
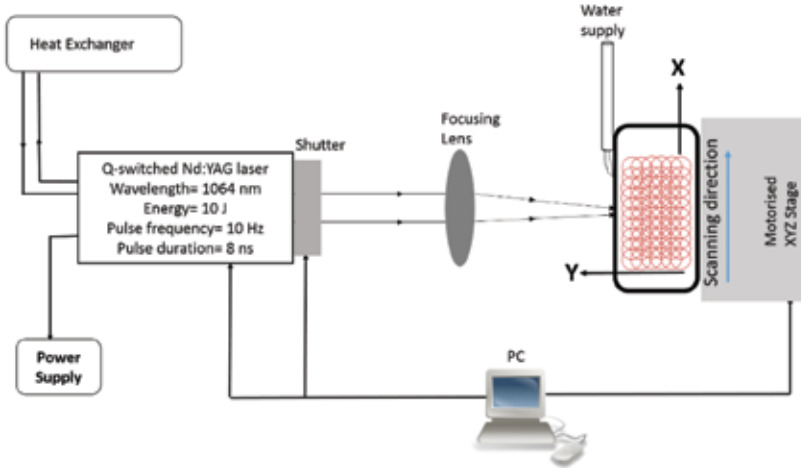
FIGURE 1
Schematic representation of laser shock peening (LSP) process.

considered to deform plastically when the shock wave pressure exceeds the Hugoniot Elastic Limit (*HEL*) of the material.

According to Fabbro *et al* [50] and Peyre *et al* [7, 8], the peak plasma pressure, P, can be expressed as

$$P(GP\alpha) = 0.01\sqrt{\frac{\alpha}{2\alpha+3}}\sqrt{Z\left(\frac{g}{cm^2 s^2}\right)}\sqrt{I_0\left(\frac{GW}{cm^2}\right)} \tag{1}$$

where, $I_0 \left(= \dfrac{P_{avg}}{f \times \tau \times A}\right)$ is the laser power density and P_{avg}, f, τ, A, Z, and α are the average power (W), pulse repetition rate (Hz), pulse duration (ns), laser spot area (cm^2), reduced shock impedance between the material and the confining medium, and efficiency of plasma-material interaction (0.1 – 0.2) [8], respectively. The importance of α during laser-material interaction is that it contributes to the total energy (E_t) by converting part of energy (αE) to thermal energy and rest of the energy ((1 - α)E) is used to generate and ionize plasma. The increased in thermal energy increases the pressure of the plasma.

The reduced shock impedance is expressed as [8]

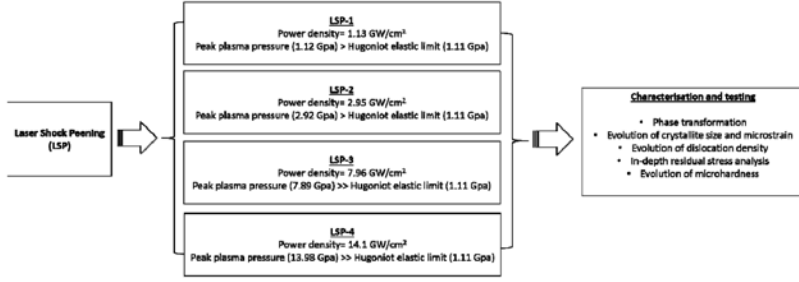$$\frac{2}{z} = \frac{1}{z_1} + \frac{1}{z_2} \tag{2}$$

FIGURE 2
Process Map For The Laser Shock Peening Of Hastelloy-X Superalloys.

where, Z_1 and Z_2 are the shock impedances of target material and confining medium, respectively. In the present study, Z_1 (nickel) = 4.14×10^6 gcm^{-2}s^{-1} and Z_2 (water) = 0.165×10^6 g.cm^{-2}.s^{-1} [20].

The reduced shock impedance according to Equation. (2) is measured to be 0.32×10^6 g.cm^{-2}.s^{-1}. The value of peak pressure developed on the sample's surface following LSP was calculated according to Equation. (1) is shown in Figure. 2. The *HEL* of any material is related to its dynamic yield strength (σ_{Ydyn}) as [6, 45]

$$HEL = \frac{1 - \vartheta}{1 - 2\vartheta} \sigma_Y^{dyn} \tag{3}$$

where, υ is the Poisson's ratio of the material. The value of σ_Y^{dyn} was taken from ref. [45] for the calculation of *HEL*. The calculated value of *HEL* was measured using Equation. (3) and is shown in Figure. 2.

The laser shock peening parameters were chosen to ensure that the peak plasma pressure exceeds the *HEL* of the material to plastically deform the material.

2.3 Material characterization

2.3.1 Phase analysis

X-ray diffraction (XRD) (D8 Discover; Bruker Corporation) was used to study the phase evolution following LSP using a Cu Kα radiation with a scan step of of 0.02°/s and time per step of 0.1 s. For the measurement of full width at half maximum (FWHM) of the diffraction peaks, scanning speed of 0.01°/s and time per step of 5 s were employed to ensure higher peak counts. Each peak was then fitted using Pseudo-Voight function with Origin8.5 software platform.

The Williamson-Hall method for Uniform Stress Deformation Model (USDM) considering the anisotropic nature of the strain was used for the determination of microstrain developed in the crystal lattice following LSP. The equation used to calculate the microstrain is presented below [51, 52].

$$\beta_{hkl} cos\theta_{hkl} = \frac{k\lambda}{D} + 4\left(\frac{\sigma}{E_{hkl}}\right)sin\,\theta_{hkl} \tag{4}$$

where, β is the full width half maximum (FWHM), θ is the diffraction angle, K ($\approx$ 1) is a constant, λ is the X-ray wavelength, and D is the crystallite size (or domain size). The suffix, hkl, refers to a crystallographic plane.

From the slope and intercept of the plot between β_{hkl} $cos\theta$ and $4sin\theta/E_{hkl}$, the lattice deformation stress, σ, and the crystallite size, D, were measured, respectively.

The microstrain *(ε) can be re-written as* $\left(\varepsilon^{hkl} = \frac{\sigma}{E_{hkl}}\right)$, where E_{hkl} is the Young's modulus in a crystallographic direction perpendicular to the lattice plain (hkl).

2.3.2 Microstructural analysis
Optical microscopy of the LSP treated surface was carried out using a light optical microscope (Axio Observer; ZIESS) to measure the grain size. The grain size was measured using linear intercept method according to ASTM E112 – 13. Microstructural analysis of the LSP treated surface was carried out using scanning electron microscope (SEM) (Gemini SEM; ZIESS). The samples were chemical etched prior to microstructural study. The etchant used to etch Hastelloy-X samples was Waterless Kalings reagent. The etching time was optimized to be 30 seconds for Hastelloy-X samples.

2.3.3 Dislocation density measurement
Wiliamson and Smallman method [53] was used to measure dislocation density in untreated and LSP treated samples. The method assumes the crystallite size and microstrain are related to dislocation density as:

$$\rho = \frac{2\sqrt{3}\left\langle\varepsilon^2\right\rangle^{1/2}}{Db} \tag{5}$$

where, $<\epsilon^2>^{1/2}$ is the root mean square (rms) microstrain, D is the size of coherently diffracting domains, and b is the burger vector in <110> direction and for an FCC crystal it is expressed as b= <110> a/2, where a is the lattice

parameter. The lattice parameter was measured using XRD and it was to be 0.355 nm for Hastelloy-X superalloy.

2.3.4 Residual stress measurement using incremental hole drilling technique

The incremental hole drilling technique was used to measure residual stress along the depth of the sample. The measurement was carried out using a hole drilling apparatus (Restan-MTS3000; SINT Technologies) which consists of both the mechanical and electronic drills. For this study here, the electrical drill was employed. The obtained data was then evaluated by a control software (RMS) and back calculation software (EVAL). The drilling device was mounted using magnetic feet on a 12 mm thick mild steel plate. The identification of the surface of the sample (reference point for drilling) was controlled by the electrical contact between the endmill and the metallic sample. The end mill diameter was 1.5 mm. The drilling speed was kept at 0.1 mm/min. The acquisition delay and the drilling delay were kept at 4s and 3s, respectively. The residual stresses were calculated by the HDM method using the constant spline function with eccentricity correction between the drilled hole and the center of the strain gage rosette.

2.3.5 Microhardness Measurement

Vickers microhardness tester (DURASCAN-70; Struers) was used to measure the hardness of untreated and LSP treated samples using 100 gf load and a dwelling time of 10 seconds.

3. RESULTS

3.1 Microstructural characterisation

Figure. 3 shows the optical micrographs of (a) LSP-1, (b) LSP-2, (c) LSP-3, (d) LSP-4, and (e) unpeened sample. Surface microstructure modification is evident from the cross-section of optical micrographs following LSP. The depth of microstructural modification varies between 40 to 90 mm as shown by the dotted lines. Higher depth of microstructural modification can be observed for sample treated with a peak power density of 14.1 GW/cm^2 (LSP-4). The grain sizes were measured on three different samples using linear intercept method (ASTM E112 – 13) and the lowest grain size of 23 mm (± 1.5 mm) was measured for LSP-4 (14.1 GW/cm^2). The measured grain size for LSP-1 (1.12 GW/cm^2), LSP-2 (2.95 GW/cm^2), and LSP-3 (7.96 GW/cm^2) were 30 mm (± 2.8 mm), 28 mm (± 2.3 mm), and 25 mm (± 1.8 mm), respectively. The measured grain size in an unpeened sample was 57 mm (± 5.2 mm).
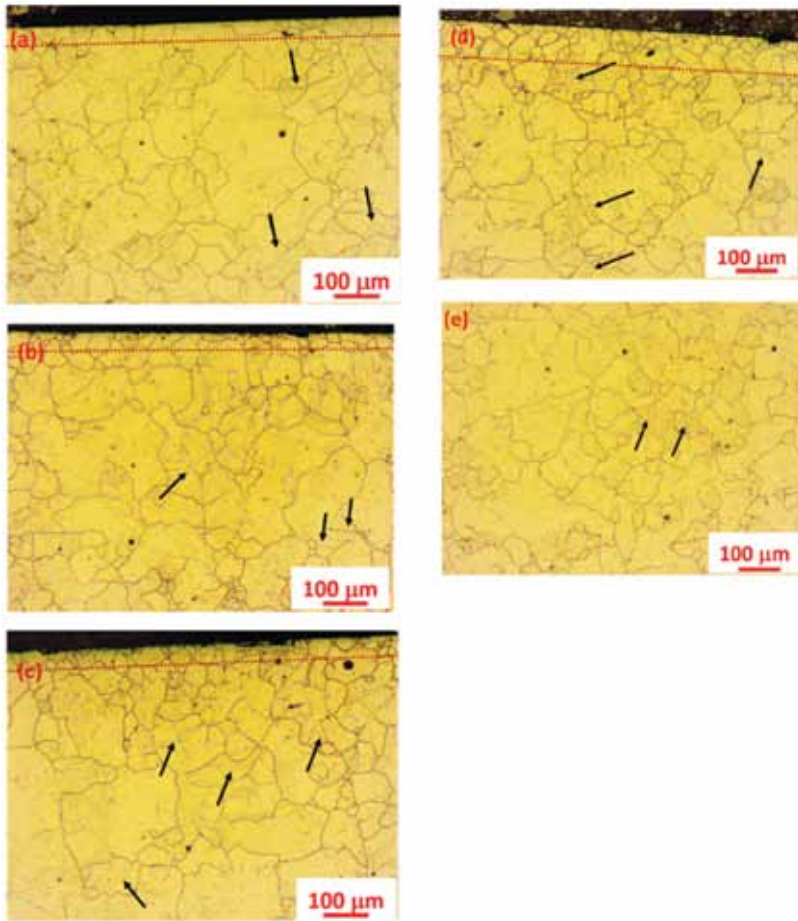
FIGURE 3

Cross-sectional optical micrographs of (a) LSP-1, (b) LSP-2, (c) LSP-3, (d) LSP-4, and (e) unpeened sample.

Figure. 4 shows the scanning electron micrograph of the cross-section of (a) LSP-1, (b) LSP-2, (c) LSP-3, and (d) LSP-4. From Figure. 4 (a-d), the deformation induced grain size reduction is evident. Hastelloy-X is a solid solution strengthened Ni-Fe superalloy. Presence several annealing twins in the austenitic matrix is evident in the microstructure of the Hastelloy-X superalloys which formed due to solution annealing treatment of samples to relieve any trapped stress before LSP.

High magnification scanning electron micrographs of an unpeened sample (Figure. 5a) and LSP-4 (Figure. 5b) are shown in Figure. 5. The high magnification micrographs don't show any sign of significant microstructural refinement with only presence of sub-grains (as shown by arrows) in a grain
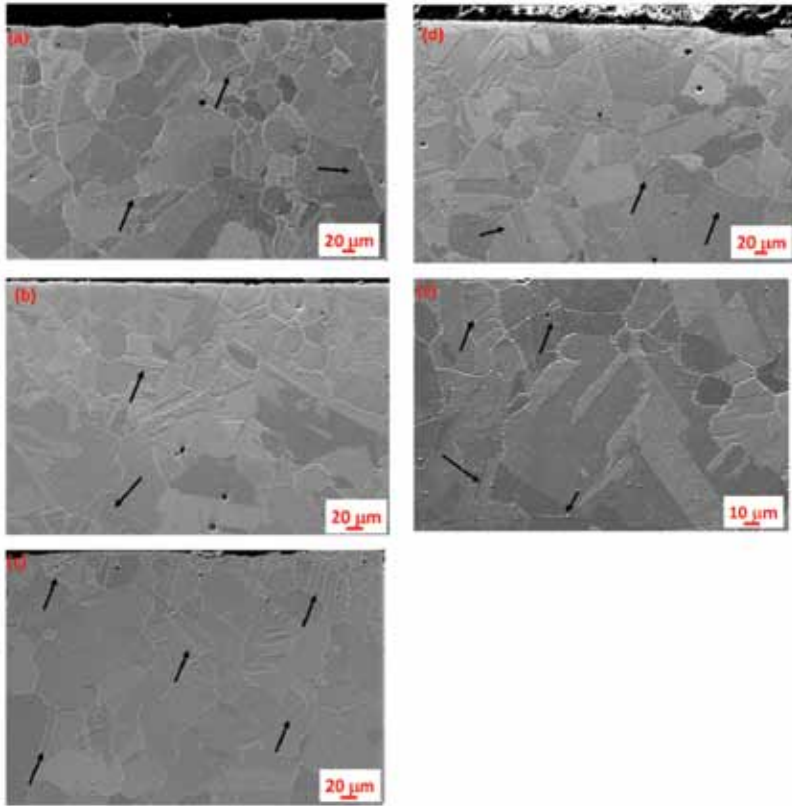
FIGURE 4

Cross-sectional scanning electron micrographs of (a) LSP-1, (b) LSP-2, (c) LSP-3, (d) LSP-4, (e) unpeened sample.

as shown in Figure. 5b with the dotted line. No evidence of surface melting is also observed in Figure. 5b which confirms the process was purely mechanical without any thermal effect.

3.2 Phase analysis

Figure. 6 shows the XRD phase scans of an untreated Hastelloy-X superalloy (plot 1), LSP-1 (plot 2), LSP-2 (plot 3), LSP-3 (plot 3), and LSP-4 (plot 5). The XRD phase scans reveal presence of face centered cubic (FCC) reflections of nickel (Ni) matrix in both untreated and laser shock peened samples. There is no trace of reflections from any other phase suggesting that there was no separate phase formation (oxides) or phase transformation due to high pressure shock waves during LSP which corroborates microstructural studies indicating absence of melting (no thermal effect). The lattice parameter in the unpeened and LSP treated Hastelloy-X samples were measured to be 0.355
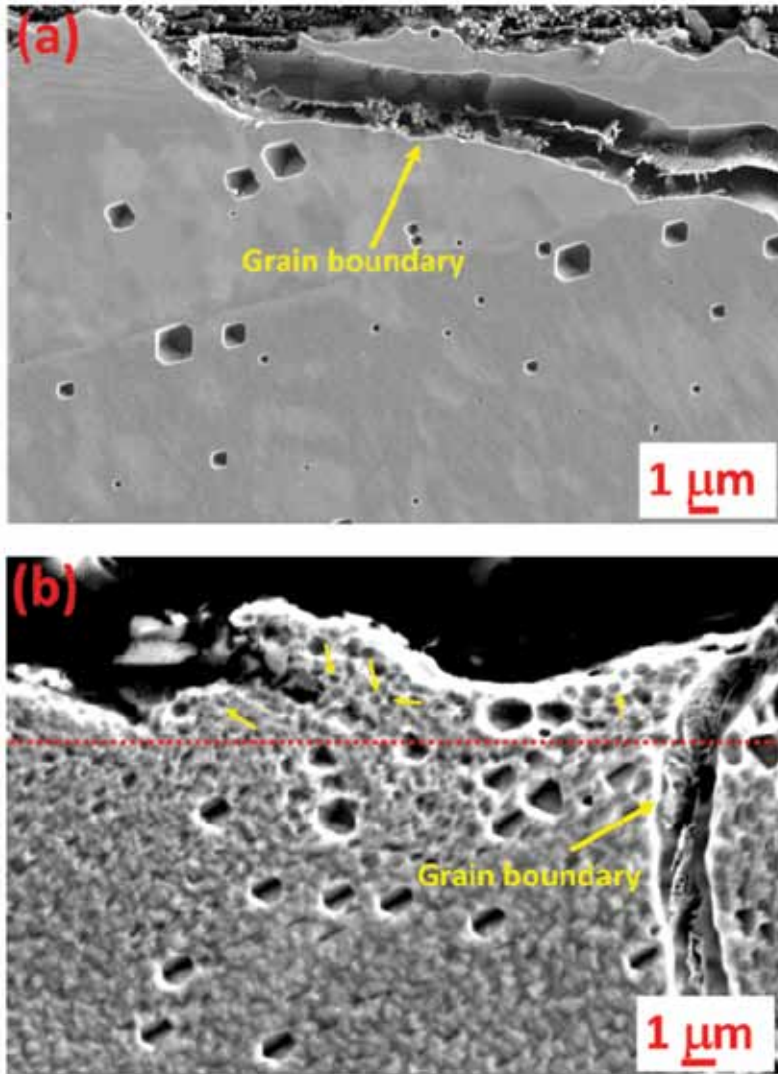
FIGURE 5
Scanning electron micrographs of cross-section of (a) as-received Hastelloy-X and (b) LSP-4.

nm which was used to calculate burger vector in the <110> direction and hence, the dislocation density.

The crystallite size (D) and *rms* microstrain (ϵ_{rms}) in laser shock peened samples were estimated from the XRD peak broadening using Uniform Stress Deformation Model (USDM) and the estimated values are plotted in Figure. 7. It should be noted here that, D is the size of the homogeneous domains contributing to coherent diffraction under XRD, and is less than the grain
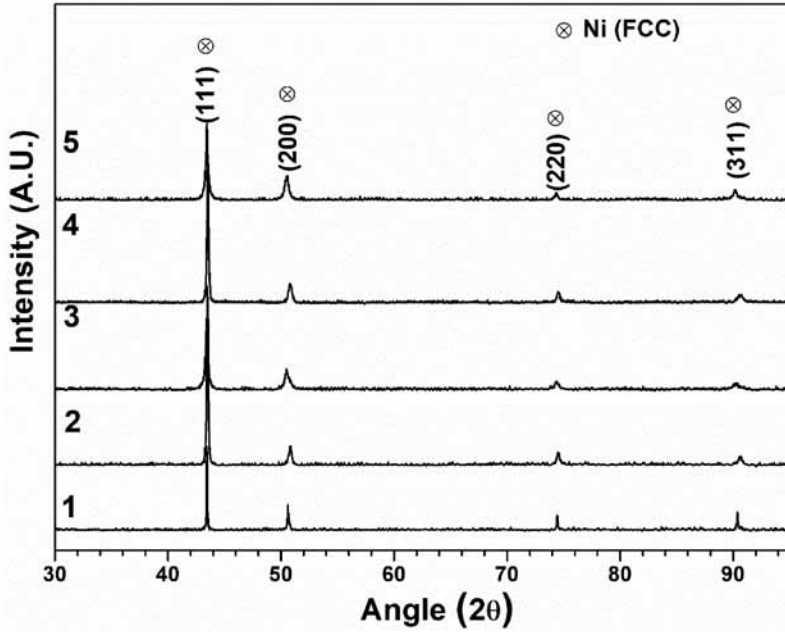
FIGURE 6
X-ray diffraction scans of an untreated hastelloy x superalloy (plot 1), LSP-1 (plot 2), LSP-2 (plot 3), LSP-3 (plot 3), and LSP-4 (plot 5).
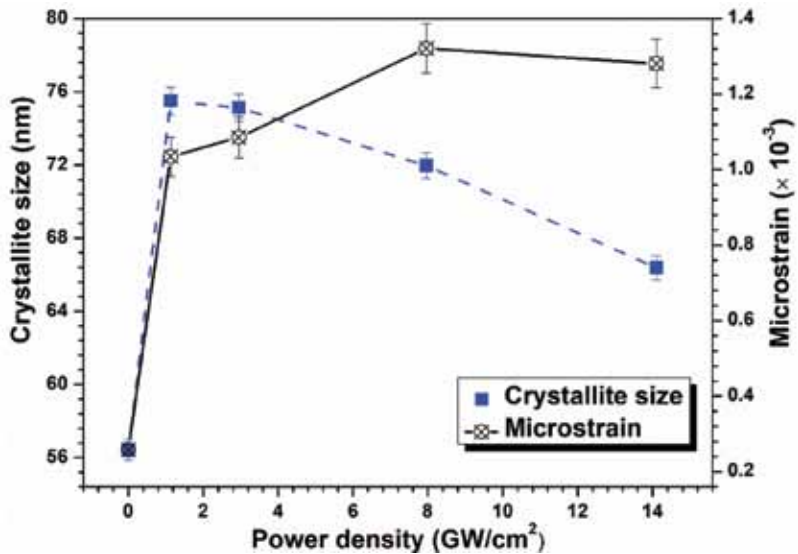

FIGURE 7
Variation of crystallite size and microstrain with laser power density.

size, which was estimated by optical microscopy and scanning electron microscopy. On the other hand, dislocations are considered to be the line defects which are responsible for the peak shift, broadening and asymmetry in the XRD pattern. The measurement and analysis of dislocation density and peak broadening are discussed in the following sections. The crystallite size of an untreated Hastelloy-X superalloy was measured to be 56 nm. It is interesting to note that with the application of LSP surface treatment the crystallite size increases which is evident from Figure. 7. The crystallite sizes of LSP-1, LSP-2, LSP-3, and LSP-4 were measured to be 76 nm, 75 nm, 72 nm, and 66 nm, respectively. From Figure. 7, it can be observed that the crystallite size decreases with increase in the laser power density which implies that higher the plastic deformation, the lower is the crystallite size. The root mean square (*rms*) microstrains were measured using the microstrains observed in different crystallographic directions. Figure. 7 shows the *rms* microstrain developed on the laser shock peened samples. The microstrain measured in the Hastelloy-X samples were also found to be dependent on the laser power density. With the increase in the laser power density, the microstrain developed on the surface of the sample increases as shown in Figure. 7.

Figure. 8 shows the variation of dislocation density with laser power density. Measuring dislocation density in laser shock peened samples is an effective way to quantify plastic deformation. High strain rate surface plastic deformation of the metallic systems were reported to increase the dislocation
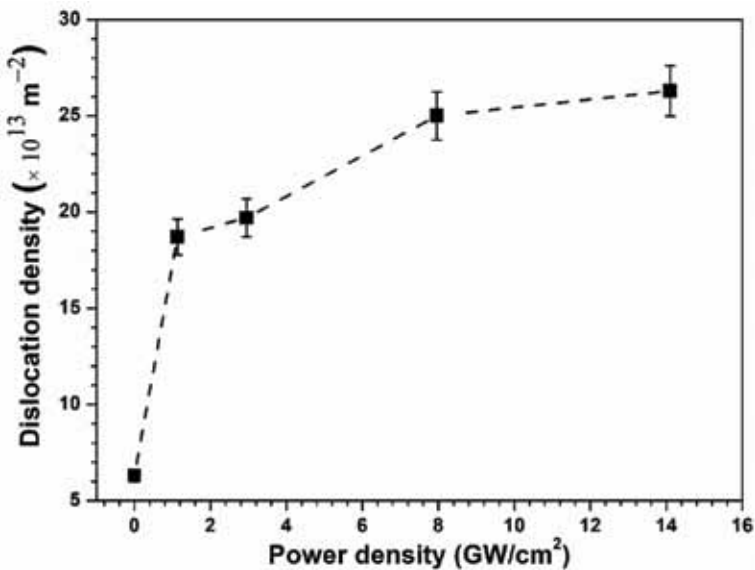

FIGURE 8
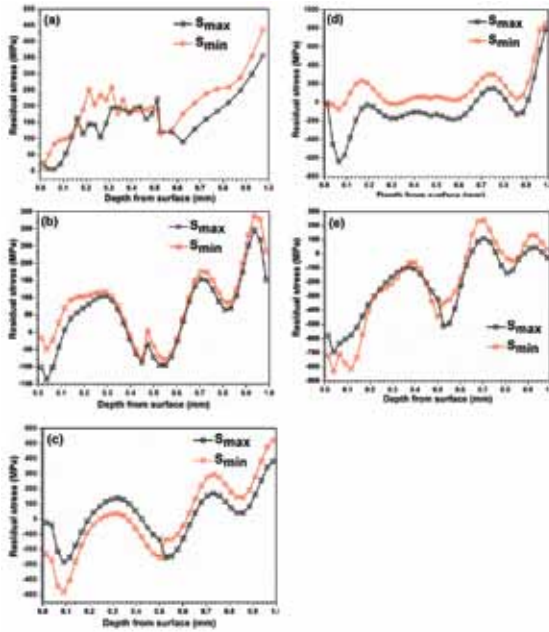Variation of dislocation density with laser power density.

FIGURE 9
Incremental hole drilling residual stress measurement of (a) as-received Hastelloy-X sample, (b) LSP-1, (c) LSP-2, (d) LSP-3, and (4) LSP-4.

density which resulted in surface hardening as well as formation of nano-structured zone on the surface [24, 54]. From Figure. 8, it may be noted that the dislocation density in an untreated sample is 6.3×10^{13} m^{-2} which increases to a maximum value of 26.3×10^{13} m^{-2} for LSP-4. The dislocation density in LSP-1, LSP-2, and LSP-3 were measured to be 18.7×10^{13} m^{-2}, 19.7×10^{13} m^{-2}, and 25×10^{13} m^{-2}, respectively.

3.3 Incremental hole drilling

LSP is a process where plastic loading and unloading takes place which leads to the development of compressive residual stress in the material. Residual stress distributions in the untreated and LSP treated samples as a function of depth are shown in Figure. 9 (a-e). Stresses were measured in two directions perpendicular to each other. The initial stress on the untreated sample's surface is tensile in nature (S_{max}= 23 MPa and S_{min}= 9 MPa) as shown in Figure. 9 (a). From Figure. 9 (b-e), it can be observed that the LSP treated samples shows development of compressive residual stress following LSP and the maximum compressive residual stress was measured just below the surface. The compressive nature of the residual stress developed on the samples following LSP confirms the theoretical

data shown in Figure. 2. It is to be noted that the depth of compressive residual stresses in LSP-1 to LSP-4 varies between 0.1 mm to 0.35 mm. The previous studies have shown the depth of compressive stress is extended up to 1 mm [24, 54, 55]. The difference in depth of compressively stressed zone in the present study and previous studies may be attributed to the use single shot laser pulse instead of multiple shots [55]. This is because of the work hardening of the material due to dislocations generation in first shot which then decreases the rate of attenuation of the subsequent pressure pulse followed by a higher peak pressure to deform deeper into the material on successive shots. The compressive residual stress components S_{max} and S_{min} for LSP-1 were measured to be 140 MPa and 50 MPa, respectively as shown in Figure. 9 (b). Residual compressive stress components for LSP-2 were 481 MPa (S_{max}) and 280 MPa (S_{min}) as shown in Figure. 9 (c). Maximum compressive residual stresses of 697 MPa (S_{max}) and 834 MPa (S_{min}) were measured at 39 mm below the surface for LSP-3 as shown in Figure. 9 (d). On the other hand, the compressive residual stresses measured for LSP-4 were 637 MPa (S_{max}) and 73 MPa (S_{min}).

4 DISCUSSION

LSP is a high strain rate deformation process which results in producing nanostructured zones in the surface microstructure. Table 2 compares the results obtained in the present study and reported works on LSP of Ni-based superalloys. These will be discussed in the following section. It is important to mention here that no other studies on LSP of Ni-based alloys have used incremental hole drilling technique to measure the residual stress through depth.

Following grain size measurements using Figure. 3 (a-d), a maximum reduction in grain size of 60% with a laser power density of 14.1 GW/cm^2 was observed. The increased shock wave pressure at higher laser power density is the reason behind the reduction in grain size. Hua *et al* [25] reported similar reduction in grain size following LSP. The reported value of grain size following LSP was 18.5 mm as compared to 33.3 mm in an untreated GH586 superalloy. The grain size reduction observed in the present study is not so significant as compared to several other studies where grain sizes were in the order of nanometer following LSP [24, 54]. However, reported studies were conducted with multiple laser shots during LSP which resulted in a grain size reduction whereas a single-shot strategy was used in the present study. Studies carried out by Trdan *et al* [19] and Kattoura *et al* [24] showed the grain size in the near surface regions were in the range of 20-50 nm following LSP Al-Mg-Si alloys and ATI 718Plus alloy, respectively. Interestingly, a laser power density of 4.7 GW/cm^2 was shown to produce a nanostructured zone

TABLE 2
Reported works on LSP of Ni-based alloys and its comparison with the present study.

Ni-based alloy	Laser energy (J)	Laser intensity (GW/cm²)	Residual stress (MPa)	Hardness	Ref.
Hastelloy-X superalloy	Wavelength = 1064 nm; Pulse energy= 8 J; Pulse duration= 8 ns; Pulse repetition rate= 10 Hz; Spot diameter= 3-7.5 mm; Overlap= 50%	1.13 - 14.1	Untreated= 23 $(S_{max})^e$ and 9 $(S_{min})^e$; LSP= 697 $(S_{max})^e$ and 834 $(S_{min})^e$	Untreated= 208 HV0.1[a], LSP= 243 HV0.1[a] (1 shot)	Present study
K403 nickel alloy	Wavelength = 1064 nm; Pulse energy= 5-25 J; Pulse duration= 20 ns; Pulse repetition rate= 1 Hz; Spot diameter= 2 mm; Overlap= 60%	12	LSP= -633 (1 shot)[d]; -826 (2 shot)[d], -882 (3 shot)[d]	Untreated= 389 HV0.3[a]; LSP= 453 HV0.3[a] (1 shot); 461 HV0.3[a] (2 shot); 475 HV0.3[a] (3 shot)	[20]
Inconel alloy 718	Wavelength = 1054 nm; Pulse energy= 1.5-3.9 J; Pulse duration= 20 ns; Spot diameter= 1.8 mm; Overlap= 50%	2.9 – 7.7	LSP= -550[d]		[21]

Material	Laser parameters		Residual stress	Hardness	Ref
Single crystal Ni-superalloy	Wavelength = 1064 nm; Pulse energy= 6 J; Pulse duration= 14 ns; Pulse repetition rate= 2 Hz; Spot diameter= 2 mm; Overlap= 0%	13.6		$\sim$ 7.1 GP[ab] ($\approx$724 HV)	[22]
Incoloy 800 superalloy	Wavelength = 1064 nm; Pulse energy= 0.4 J; Pulse duration= 10 ns; Pulse repetition rate= 10 Hz; Spot diameter= 3 - 6 mm		LSP= -227[d]	201 HV0.3[a]	[23]
ATI 718 Plus superalloy	Wavelength = 1064 nm; Pulse energy= 3 J; Pulse duration= 20 ns; Pulse repetition rate= 10 Hz; Spot diameter= 2 mm; Overlap= 50%	4.7	Untreated= -160 (X)[d] and -69 (Y)[d]; LSP= -746 (X)[d] and -695 (Y)[d]	Untreated= 6.71 GP[ab] ($\approx$ 684 HV); LSP= 8.33 GP[ab] ($\approx$ 849 HV)	[24]
GH586 superalloy	Wavelength = 1064 nm; Pulse energy= 15 J; Pulse duration= 30 ns; Spot diameter= 4 mm; Overlap= 50%			LSP= $\sim$510.3 HV0.2[a]	[25]
Inconel 718 SPF superalloy	Wavelength = 1054 nm; Pulse energy= 8.23 and 15.24 J; Pulse duration= 28.6 and 25.3 ns; Spot diameter= 2 and 2.18 mm; Overlap= 50%	9 and 16	LSP= -750 (at 8 J)[d] and -690 (at 16 J)[d]	LSP= $\sim$322 HK0.05[c]	[26]
Astroloy superalloy	Wavelength = 1064 nm; Pulse energy= 80 J; Pulse duration= 25 ns; Pulse repetition rate= 1 Hz; Spot diameter= 8 mm	5	LSP= -700[d]		[27]
K417 superalloy	Wavelength = 1064 nm; Pulse energy= 8 J; Pulse duration= 20 ns; Spot diameter= 3 mm; Overlap= 33 %	11.3	LSP= -600[d]		[28]
K417 superalloy	Wavelength = 1064 nm; Pulse energy= 10.8 J; Pulse duration= 20 ns; Spot diameter= 3.4 mm; Overlap= 60 % 1 Hz;	6	LSP= -583 (1 shot)[d], -624 (3 shots)[d]	Untreated= 380 HV0.2[a], LSP= 445 HV0.2[a]	[29]

[a]Vickers Hardness; [b]Nano-hardenss; [c]Knoop Hardness; [d]X-ray diffraction; [e]Hole drilling

near the surface in Ni-based superalloys [24] whereas a laser power density of 14.1 GW/cm^2 in the present study didn't result in the formation of nano-meter sized grains in Hastelloy-X samples. No grain refinement in Inconel 718 SPF alloy was, however, observed by Gill *et al* [26] following LSP with a laser power density of 16 GW/cm^2. The reason of the observation may be related to single-shot LSP strategy. Nonetheless, with the use of single-shot LSP a significant decrease in grain size was observed which would help to fine tune the LSP process further for getting higher surface strength and improved surface properties. A transmission electron microscopy study will be done in future to measure the grain size in the near surface zone. Nonethe-less, grain size reduction is evident, however, a nanostructured zone is not evident. Comparing Figure. 5a and Figure. 5b, it may also be noted that the surface of LSP-4 is wavier than the surface of the unpeened sample. The sur-face waviness is believed to be due to the laser shock wave induced deforma-tion.

In LSP, the severity of plastic deformation increases with the increase in the peak pressure exerted on the sample. The peak plasma pressure can be controlled by exploiting the laser power density and the reduced shock impedance according to Equation. (1). Moreover, the peak plasma pressure can also be controlled by using different absorptive mediums and confining mediums [6, 56, 57]. In the present study, water was used as a confinement medium and black vinyl tape was used as an absorptive medium. However, laser power density was varied.

The increase in dislocation density in the LSP treated samples indicates an increase in the magnitude of plastic deformation which is necessary to obtain a hardened surface and to induce compressive residual stress on the surface of the superalloy. By looking at Equation. (1), it is clear that with the increase in laser power density, the peak plasma pressure on the surface increases. An increased peak plasma pressure then deforms the material by pure mechanical effect. In the present study, a 4-fold increase in the magni-tude of dislocation density was observed following LSP with a laser power density of 14.1 GW/cm^2 as shown in Figure. 8. A 2.5 times increase in dislocation density (measured using Smith–Guttman linear intercept tech-nique) was reported by Tradan *et al* [19] following LSP of aluminum alloy. It is to be noted that no reported dislocation density on Ni-based alloys fol-lowing LSP was found to compare with the present study. The increase in the dislocation density is attributed to the peak plasma pressure of 13.98 GPa (*cf.* Figure. 2) which is much higher than the *HEL* of the material ($\approx$ 1.11 GPa). Three-fold increase in the dislocation density was also observed when the sample was LSP treated with a laser power density of 1.13 GW/cm^2 as compared to the untreated sample. It is important to mention here that a laser power density of 1.13 GW/cm^2 induces a peak plasma pressure of 1.12 GPa on the surface of the sample as mentioned in Figure. 2. The minimum plasma pressure requires to induce plastic deformation in the

material is 1.11 GPa ($\approx$ *HEL*). The small difference of ~5% in the measured dislocation density between LSP-1 and LSP-2 is due to the smaller change in the laser power density in LSP-2 than in LSP-1 as shown in Figure. 8. However, a considerable increase in dislocation density of almost 27% can be observed following an increase in the laser power density from 2.95 GW/cm^2 to 7.96 GW/cm^2 as evident from Figure. 8 which is attributed to increase in peak plasma pressure. Figure. 8 also depicts that the dislocation density in LSP-4 shows a change of only ~5% as compared to LSP-3. This is almost similar to the difference between LSP-1 and LSP-2. However, the difference in laser power density between LSP-3 and LSP-4 is more as compared to the difference between LSP-1 and LSP-2. It is believed that the confinement layer breakdown phenomenon may be the reason behind the small increase in the dislocation density [6]. Confinement layer breakdown phenomenon indicates that the confining dielectric medium (water in this case) is no more transparent to the incident laser radiation due to increase in plasma in the dielectric volume and the transmission of laser radiation through the confining medium to the interface is severely disrupted by the inverse Bremsstrahlung mechanism. This behavior is characterized by saturation in plasma pressure with increase in laser power density.

The generation of compressive stress is also dependent on the applied laser power density. That is why higher values of compressive stress were measured for LSP-3 and LSP-4 as compared to LSP-1 and LSP-2 samples. It should also be noted that reported results were also shown to have tensile residual stress which is due to surface melting during LSP [21]. The reported compressive residual stress values were between -227 MPa and – 882 MPa [20, 21, 23, 24, 26-29]. The reported compressive residual stresses using single-shot LSP were 633 MPa [20] and 583 MPa [29]. The variation in the reported values and the value measured in the present study is believed to be due to the different LSP conditions/parameters employed herein. Moreover, the LSP-4 sample showed lower stress value than LSP-3 which may be due to the confinement layer break down phenomena. The confinement layer breakdown phenomena is observed when the laser power density increases to a critical value (as happened for LSP-4) beyond which the peak plasma pressure is no longer a linear function of laser power density and a scattered compressive stress may be observed beyond this point [6]. The increased compressive residual stress in Hastelloy-X superalloys following LSP surface treatment may be beneficial in improving the fatigue strength of the superalloy under study which is in scope of future study. The improvement in microhardness is related to the strain hardening phenomena which is observed following LSP surface treatment.

Figure. 10 shows the microhardness distribution in the LSP treated samples LSP-1, LSP-2, LSP-3, and LSP-4. A maximum hardness of 243 HV0.1 was measured on the surface of LSP-4. The surface hardness of LSP-1, LSP-2, and LSP-3 were measured to be 212 $HV_{0.1}$, 223 $HV_{0.1}$, and 240 $HV_{0.1}$,
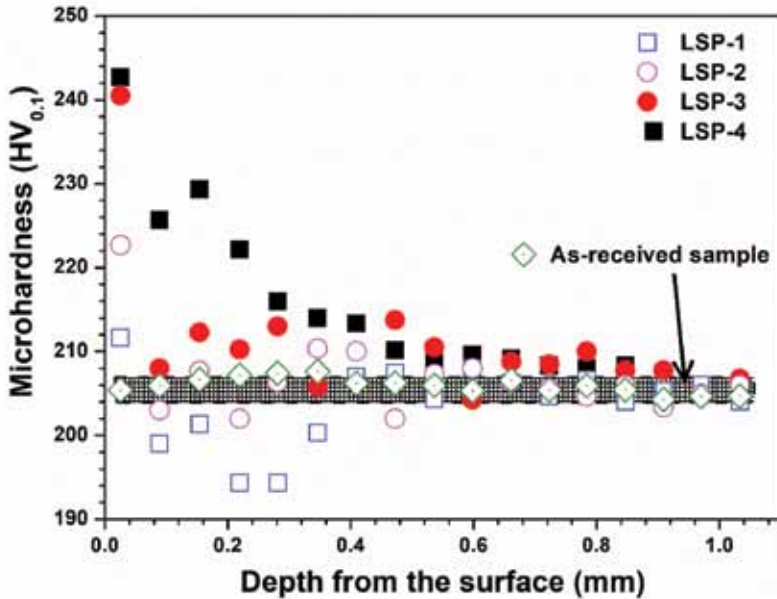
FIGURE 10

Microhardness distribution with depth in laser shock peened Hastelloy-X superalloy samples.

respectively as shown in Figure. 10. From Figure. 10, it is evident that the microhardness on the surface is higher than the interior with a gradual distribution of microhardness across its depth. From Figure. 10, the LSP surface treatment shows improved surface hardening as compared to an untreated sample. A maximum increment in hardness of ~16.8% was measured following LSP. Wang *et al* [20] found an increment in microhardness of 16.5% in K403 alloy following single-shot LSP which is close to what was measured in the present study. The depth of hardened zone is extended up to 500 mm which is greater than the value (300 mm) reported by Wang *et al* [20]. Hua *et al* [25] found an increment in microhardness of 27% and the depth of hardened zone was found to be 250 mm. A ~20% increase in the microhardness value and wide hardened zone of ~700 mm was reported by Gill *et al* [26]. A wider hardened zone may be obtained by multiple impacts at the same point during LSP. The gradual decrease in the microhardness values with depth is related to the decrease in the dislocation density with depth as shock pressure decreases as the shock waves travel from surface towards interior of the sample. The surface experiences a maximum shock pressure which goes on in a decreasing trend. The observed surface hardening phenomena is related to the increased dislocation density following LSP surface treatment (*cf.* Figure. 8). The enhanced surface hardening behavior of Hastelloy-X superalloys following LSP surface treatment would also improve the wear resistance of the

superalloy under study and should be a subject of future studies. It may be noted that there are some anomalies in the plot for LSP-2 and LSP-3 which indicates some additional mechanisms taking place here which is a subject for future study.

5 CONCLUSIONS

This investigation aims at studying the effectiveness of Laser Shock Peening (LSP) to tailor the surface properties of a new Hastelloy-X superalloys. This was done by focusing on understanding the evolution of phase, dislocation density, microstructure, surface hardening, and residual stress following LSP. A single-shot strategy was used to quantify depth of compressive residual stress following LSP. Microstructure and property analyses were undertaken to establish the mechanism of surface hardening. The investigation led to the following conclusions.

(i) Microstructural refinement and reduction in gran size were observed with single-shot LSP. The measured grain sizes were between 23 mm to 30 mm. The single-shot LSP showed ~60% reduction in grain size as compared to the untreated sample.

(ii) A maximum *rms* microstrain of 1.321×10^{-3} was measured on the surface of the Hastelloy-X. The *rms* microstrain increased with increase in the laser power density except for LSP-4 where confinement layer breakdown was believed to have occurred. Crystallite size showed a boost following LSP as compared to an untreated sample. With increase in laser power density, the crystallite size, respectively, showed a decreasing trend.

(iii) Single-shot LSP showed increase in dislocation density. A maximum dislocation density of 26.3×10^{13} m^{-2} was measured for the laser power density of 14.1 GW/cm². With increase in the laser power density, the dislocation density increased. However, the increment was within the same order of magnitude of untreated sample.

(iv) Single-shot LSP induced a maximum compressive residual stress of 850 MPa when laser shock peened with a laser power density of 7.96 GW/cm². On the other hand, a laser power density of 14.1 GW/cm² showed comparatively lower residual stress development which may be due to the confinement layer breakdown phenomena. In-depth residual stress measurement showed the depth and magnitude of compressively deformed zone varies with laser power density.

(v) The surface hardening was achieved following LSP. A maximum surface hardness of 243 HV0.1 was measured following LSP. The increased hardness of the Hastelloy-X samples following LSP will increase the

strength and wear resistance and hence, it is expected to increase the component life and reduce the repair cost although further testing and analyses are necessary.

The enhanced hardness and significantly high compressive residual stress observed in the present study would significantly contribute to the application of Hastelloy-X in a gas turbine environment as well as in high temperature gas cooled reactors where cyclic loads are prevalent.

ACKNOWLEDGEMENT

NOMENCLATURE

M^2	Beam quality factor
HEL	Hugoniot Elastic Limit (GPa)
P	Peak plasma pressure (GPa)
I_0	Laser power density (W/cm^2)
P_{avg}	Average laser power (W)
f	Pulse repetition rate (Hz)
Z	Reduced shock impedance (gcm^{-2}s^{-1})
Z_1	Reduced shock impedance of nickel (4.14×10^6 gcm^{-2}s^{-1})
Z_2	Reduced shock impedance of water (0.165×10^6 gcm^{-2}s^{-1})
A	Laser spot area (cm^2)
E	Laser energy (J)
E_t	Total available energy (J)
K	Scherer constant (≈ 1)
D	Crystallite size or domain size (nm)
hkl	Indices of a crystallographic plane
σ	Lattice deformation stress (MPa)
b	Burger vector (nm)
a	Lattice parameter (nm)
S_{max}	Maximum residual stress (MPa)
S_{min}	Minimum residual stress (MPa)

Greek symbols

α	Efficiency of laser-material interaction (0.1 – 0.2)
τ	Laser pulse duration (ns)
υ	Poisson's ratio of the material.

σ_Y^{dyn}	Dynamic Yield strength (MPa)
β	Full width half maximum (Radian)
θ	X-ray diffraction angle (°)
λ	X-ray wavelength (nm)
ε	Microstrain
ε^{hkl}	Microstrain in the *hkl* direction
$<\varepsilon^2>^{1/2}$	Root mean square microstrain
ρ	Dislocation density ($1/m^2$)

REFERENCES

[1] Sakthivel T., Laha K., Nandagopal M., Chandravathi K.S., Parameswaran P., Selvi S.P., Mathew M.D. and Mannan, S.K. Effect of temperature and strain rate on serrated flow behaviour of Hastelloy X. *Material Science and Engineering A* **534** (2012), 580-587.

[2] Kim W.G., Yin S.N., Ryu W.S. Chang J.H. and Kim S.J. Tension and creep design stresses of the "Hastelloy-X" alloy for high-temperature gas cooled reactors. *Material Science and Engineering A* **483/484** (2008), 495-497.

[3] Lee J.W. and Kuo Y.C. A study on the microstructure and cyclic oxidation behavior of the pack aluminized Hastelloy X at 1100 °C. *Surface and Coatings Technology* **201** (2006), 3867-3871.

[4] Mizokami Y., Igari T., Kawashima F., Sakakibara N., Tanihira M., Yuhara T. and Hiroe T. Development of structural design procedure of plate-fin heat exchanger for HTGR. *Nuclear Engineering Design* **255** (2013), 248-262.

[5] Cho H., Lee D.M., Lee J.H., Bang K.H. and Lee B.W. Thermal oxidation behavior of ceramic-coated Ni–Cr-base superalloys. *Surface and Coatings Technology* **202** (2008), 5625-5628

[6] Ding K. and Ye L. *Laser Shock Peening Performance and Process Simulation*. Cambridge: Woodhead Publishing. 2006.

[7] Peyre P. and Fabbro R. Laser shock processing: a review of the physics and applications. *Optical and Quantum Electronics* **27** (1995), 1213-1229.

[8] Peyre P., Fabbro R., Merrien P. and Lieurade H.P. Laser shock processing of aluminium alloys. Application to high cycle fatigue behaviour. *Material Science and Engineering A* **210** (1996), 102-113.

[9] Lu J.Z., Qi H., Luo K.Y., Luo M. and Cheng X.N. Corrosion behaviour of aisi 304 stainless steel subjected to massive laser shock peening impacts with different pulse energies. *Corrosion Science* **80** (2014), 53–59.

[10] Lim H., Kim P., Jeong H. and Jeong S. Enhancement of abrasion and corrosion resistance of duplex stainless steel by laser shock peening. *Journal of Materials Processing Technology* **212** (2012), 1347– 1354.

[11] Montross C.S., Wei T., Ye L., Clark G. and Mai Y.W. Laser shock processing and its effects on microstructure and properties of metal alloys: A review. *International Journal of Fatigue* **24** (2002), 1021–1036.

[12] Rubio-González C., Felix-Martinez C., Gomez-Rosas G., Ocana J.L. Morales M., and Porro J.A. Effect of laser shock processing on fatigue crack growth of duplex stainless steel. *Material Science and Engineering A* **528** (2011), 914–919.

[13] Shukla P., Nath S., Wang W., Shen X. and Lawrence J. Surface property modifications of silicon carbide ceramic following laser shock peening. *Journal of the European Ceramic Society* **37** (2017), 3027-3038.

[14] Shukla P., Robertson S., Wu H., Telang A., Kattoura M., Nath S., Mannava S.R., Vasudevan V.K. and Lawrence J. Surface engineering alumina armour ceramics with laser shock peening. *Materials Design* **134** (2017), 523-538.

[15] Kashaev N., Ventzke V., Horstmann M., Chupakhin S., Riekehr S., Falck R., Maawad E., Staron P., Schell N. and Huber N. Effects of laser shock peening on the microstructure and fatigue crack propagation behaviour of thin AA2024 specimens. *International Journal of Fatigue* **98** (2017), 223-233.

[16] Salimianrizi A., Foroozmehr E., Badrossamay M. and Farrokhpour H. Effect of laser shock peening on surface properties and residual stress of Al6061-T6. *Optics and Lasers in Engineering* **77** (2016), 112-117.

[17] Luo K.Y., Lin T., Dai F.Z., Luo X.M. and Lu J.Z. Effects of overlapping rate on the uniformities of surface profile of LY2 Al alloy during massive laser shock peening impacts. *Surface and Coatings Technology* **266** (2015), 49-56.

[18] Trdan U. and Grum J. SEM/EDS Characterization of laser shock peening effect on localized corrosion of Al alloy in a near natural chloride environment. *Corrosion Science* **82** (2014), 328-338.

[19] Trdan U., Skarba M. and Grum J. Laser shock peening effect on the dislocation transitions and grain refinement of Al–Mg–Si alloy. *Materials Characterization* **97** (2014), 57-68.

[20] Wang C., Shen X.J., An Z.B., Zhou L.C. and Chai, Y. Effects of laser shock processing on microstructure and mechanical properties of K403 nickel-alloy. *Materials & Design* **89** (2016), 582–588.

[21] Gill A.S., Telang A. and Vasudevan V.K. Characteristics of surface layers formed on Inconel 718 by laser shock peening with and without a protective coating. *Journal of Materials Processing Technology* **225** (2015), 463–472.

[22] Lu G.X., Liu J.D., Qiao H.C., Zhou Y.Z., Jin T., Zhao J.B., Su X.F. and Hu Z.Q. Surface nano-hardness and microstructure of a single crystal nickel base superalloy after laser shock peening. *Optics and Lasers in Engineering* **91** (2017), 116–119.

[23] Amini S., Dadkhah M. and Teimouri R. Study on laser shock penning of Incoloy 800 super alloy. *Optik* **140** (2017), 308–316.

[24] Kattoura M., Mannava S.R., Qian D. and Vasudevan V.K. Effect of laser shock peening on residual stress, microstructure and fatigue behavior of ATI 718Plus alloy. *International Journal of Fatigue* **102** (2017), 121–134.

[25] Hua Y., Rong Z., Ye Y., Chen K., Chen R., Xue Q. and Liu H. Laser shock processing effects on isothermal oxidation resistance of GH586 superalloy. *Applied Surface Science* **330** (2015), 439–444.

[26] Gill A., Telang A., Mannava S.R., Qian D., Pyoun Y.S., Soyama H., Vasudevan V.K. Comparison of mechanisms of advanced mechanical surface treatments in nickel-based superalloy. *Material Science and Engineering A* **576** (2013), 346–355.

[27] Forget P., Jeandin M. and Lyoret A. Determination of laser shock treatment conditions for fatigue testing of Ni-based superalloys. *Journal de Physique IV* **3** (1993), 921-926.

[28] Zhou W.F., Ren X.D., Ren Y.P., Xu S.D., Huang J.J. and Yang T. Laser shock processing on Ni-based superalloy K417 and its effect on thermal relaxation of residual stress. *The International Journal of Advanced Manufacturing Technology* **88** (2017), 675-681.

[29] Li Y., Zhou L., He W., He G., Wang X., Nie X., Wang B., Luo S. and Li Y. The strengthening mechanism of a nickel-based alloy after laser shock processing at high temperatures. *Science and Technology of Advanced Materials* **14** (2013), 055010-055019.

[30] Kumar D., Akhtar S.N., Patel A.K., Ramkumar J. and Balani K. Tribological performance of laser peened Ti–6Al–4V. *Wear* **322/323** (2015), 203-217.

[31] Hongchao Q. Experimental investigation of laser peening on Ti17 titanium alloy for rotor blade applications. *Applied Surface Science* **351** (2015), 524-530.

[32] Hongchao Q., Jibin Z., Gongxuan Z. and Yu G. Effects of laser shock peening on microstructure and residual stress evolution in Ti–45Al–2Cr–2Nb–0.2B alloy. *Surface and Coatings Technology* **276** (2015), 145-151.

[33] Zhou Z., Bhamare S., Ramakrishnan G., Mannava S.R., Langer K., Wen Y., Qian D., Vasudevan V.K. Thermal relaxation of residual stress in laser shock peened Ti–6Al–4V alloy. *Surface and Coatings Technology* **206** (2012), 4619-4627.

[34] Cellard C., Retraint D., François M., Rouhaud E. and Le Saunier D. Laser shock peening of Ti-17 titanium alloy: Influence of process parameters. *Material Science and Engineering A* **532** (2012), 362-372.

[35] Shen X., Shukla P., Nath S., Lawrence J. Improvement in mechanical properties of titanium alloy (Ti-6Al-7Nb) subject to multiple laser shock peening. *Surface and Coatings Technology* **327** (2017), 101-109.

[36] Yella P., Venkateswarlu P., Buddu R.K., Vidyasagar D.V., Sankara Rao K.B., Kiran P.P. and Rajulapati K.V. Laser shock peening studies on SS316LN plate with various sacrificial layers. *Applied Surface Science* **435** (2018), 271-280.

[37] Hoppius J.S., Kukreja L.M., Knyazeva M., Pöhl. F. Walther F., Ostendorf A. and Gurevich, E.L. On femtosecond laser shock peening of stainless steel AISI 316. *Applied Surface Science* **435** (2018), 1120-1124.

[38] Zheng L., Zhang C., Zhang C., Dai F. Performance of micro-dent array fabricated by laser shock peening on the surface of A304 stainless steel. *Vacuum* **138** (2017), 93-100.

[39] Spadaro L., Gomez-Rosas G., Rubio-González C., Bolmaro R., Chavez-Chavez A. and Hereñú S. Fatigue behavior of superferritic stainless steel laser shock treated without protective coating. *Optics and Lasers in Engineering* **93** (2017), 208-215.

[40] Halilovič M., Issa S., Wallin M., Hallberg H. and Ristinmaa M. Prediction of the Residual State in 304 Austenitic Steel after Laser Shock Peening – Effects of Plastic Deformation and Martensitic Phase Transformation. *International Journal of Mechanical Sciences* **111/112** (2016), 24-34.

[41] Ge M., Xiang J., Fan Z., Lu Y.L. and Lei W.N. Effect of laser energy on microstructure of Mg-3Al-1Zn alloy treated by LSP. *Journal of Alloys and Compounds* **734** (2018), 266-274.

[42] Ren X.D., Huang J.J., Zhou W.F., Xu S.D., Liu F.F. Surface nano-crystallization of az91d magnesium alloy induced by laser shock processing. *Materials & Design* **86** (2015), 421-426.

[43] Liu L., Wang J. and Zhou J. Effects of laser shock peening on mechanical behaviors and microstructural evolution of brass. *Vacuum* **148** (2018), 178-183.

[44] Trdan U. and Grum J. Evaluation of corrosion resistance of AA6082-T651 aluminium alloy after laser shock peening by means of cyclic polarisation and EIS methods. *Corrosion Science* **59** (2012), 324-333.

[45] Abotula S., Shukla A. and Chona R. Dynamic constitutive behavior of Hastelloy X under thermo-mechanical loads. *Journal of Material Science* **46** (2011), 4971–4979.

[46] Shukla P.P., Lawrence J. The influence of brightness whilst laser surface processing of a silicon nitride engineering ceramic. *Optics and Lasers in* Engineering **50** (2012), 1746-17512.

[47] Shukla P.P. and Lawrence J. Role of laser beam radiance in different ceramic processing: a two wavelength comparison. *Optics and Lasers in* Engineering **54** (2013), 380 – 388.

[48] Shukla P., Lawrence J. and Zhang Yu. Understanding laser-beam brightness: a review on a new prospective in materials processing. *Optics and Lasers in* Engineering **75** (2015), 40 – 51.

[49] Shukla P.P. and Lawrence J. Identification of optical parameters for determination of radiance. *Journal of Optics* **44** (2015), 12-19

[50] Fabbro R., Fournier J., Ballard P., Devaux D. and Virmont J. Physical study of laser-produced plasma in confined geometry. *Journal of Applied Physics* **68** (1990), 775–784.

[51] Suryanarayana C. and Norton M.G. *X-Ray Diffraction: A Practical Approach*. New York: Springer 1998.

[52] Khorsand Zak A., Majid W.H.Abd., Abrishami M.E. and Yousefi R. X-Ray analysis of zno nanoparticles by Williamson–Hall and size–strain plot methods. *Solid State Science* **13** (2011), 251-256.

[53] Williamson G.K. and Smallman R.E. Dislocation densities in some annealed and cold worked metals from measurements on the X-ray Debye-Scherrer spectrum. *Philosophical Magazine* **1** (1956), 34-46.

[54] Shadangi Y., Chattopadhyay K., Rai S.B. and Singh V. Effect of LASER shock peening on microstructure, mechanical properties and corrosion behavior of interstitial free steel. *Surface and Coatings Technology* **280** (2015), 216–224.

[55] Gujba A.K. and Medraj M. Laser peening process and its impact on materials properties in comparison with shot peening and ultrasonic impact peening. *Materials* **7** (2014), 7925-7974.

[56] Fairand B.P. and Clauerthe A.H. Effect of water and paint coatings on magnitude of laser-generated shocks. *Optics Communication* **18** (1976), 588-591.

[57] Hong X., Wang S., Guo D., Wu H., Wang J., Dai Y., Xia X. and Xie Y. Confining medium and absorptive overlay: their effects on a laser-induced shock wave. *Optics and Lasers in Engineering* **29** (1998), 447-455.